Modeling long term Enhanced in situ Biodenitrification and induced heterogeneity in column experiments under different feeding strategies

Rodríguez-Escales, Paula; Folch, Albert; van Breukelen, Boris M.; Vidal-Gavilan, Georgina; Sanchez-Vila, Xavier

DOI
10.1016/j.jhydrol.2016.04.012

Publication date
2016

Document Version
Accepted author manuscript

Published in
Journal of Hydrology

Citation (APA)
Rodríguez-Escales, P., Folch, A., van Breukelen, B. M., Vidal-Gavilan, G., & Sanchez-Vila, X. (2016). Modeling long term Enhanced in situ Biodenitrification and induced heterogeneity in column experiments under different feeding strategies. *Journal of Hydrology*, *538*, 127-137. https://doi.org/10.1016/j.jhydrol.2016.04.012

Modelling long term Enhanced *in situ* Biodenitrification and induced heterogeneity in column experiments under different feeding strategies

Paula Rodríguez-Escales[1,2*], Albert Folch[1,3], Boris M. van Breukelen[4], Georgina Vidal-Gavilan[2,5], Xavier Sanchez-Vila[1]

[1]Hydrogeology Group (GHS), Department of Civil and Environmental Engineering, Universitat Politècnica de Catalunya (UPC), c/Jordi Girona 1-3, 08034 Barcelona, Spain.

[2]d D'ENGINY biorem S.L., C. Madrazo 68, 08006 Barcelona, Spain.

[3]Institut de Ciència i Tecnologia Ambientals (ICTA), Universitat Autònoma de Barcelona (UAB), Bellaterra, Barcelona 08193, Spain

[4]Department of Water management, Faculty of Civil Engineering and Geosciences, Delft University of Technology, Stevinweg 1, Delft, The Netherlands.

[5]Grup de Mineralogia Aplicada i Geoquímica de Fluïds, Departament de Cristal·lografia, Mineralogia i Dipòsits Minerals, Facultat de Geologia, Universitat de Barcelona, Martí Franquès s/n, 08028, Barcelona, Spain.

***Corresponding author:** paula.rodriguez.escales@upc.edu

Abstract

Enhanced *In situ* Biodenitrification (EIB) is a capable technology for nitrate removal in subsurface water resources. Optimizing the performance of EIB implies devising an appropriate feeding strategy involving two design parameters: carbon injection frequency and C:N ratio of the organic substrate nitrate mixture. Here we model data on the spatial and temporal evolution of nitrate (up to 1.2 mM), organic carbon (ethanol), and biomass measured during a 342 day-long laboratory column experiment (published in Vidal-Gavilan et al., 2014). Effective porosity was 3% lower and dispersivity had a seven-fold increase at the end of the experiment as compared to those at the beginning. These changes in transport parameters were attributed to the development of a biofilm. A reactive transport model explored the EIB performance in response to daily and weekly feeding strategies. The latter resulted in significant temporal variation in nitrate and ethanol concentrations at the outlet of the column. On the contrary, a daily feeding strategy resulted in quite stable and low concentrations at the outlet and complete denitrification. At intermediate times (six months of experiment), it was possible to reduce the carbon load and consequently the C:N ratio (from 2.5 to 1), partly because biomass decay acted as endogenous carbon to respiration, keeping the denitrification rates, and partly due to the induced dispersivity caused by the well-developed biofilm, resulting in enhancement of mixing between the ethanol and nitrate and the corresponding improvement of denitrification rates. The inclusion of a dual-domain model improved the fit at the last days of the experiment as well as in the tracer test performed at day 342, demonstrating a potential transition to anomalous transport that may be caused by the development of biofilm. This modeling work is a step forward to devising

optimal injection conditions and substrate rates to enhance EIB performance by minimizing the overall supply of electron donor, and thus the cost of the remediation strategy.

1 Introduction

Nitrate is a priority environmental pollutant in many countries due to the combination of high toxicity and widespread presence (European Environment Agency, 2007; Organisation for Economic Co-operation and Development, 2008). Agricultural leaching has been identified as the primary source of groundwater nitrate contamination (Böhlke, 2002; Jahangir et al., 2012). Additional sources of nitrate pollution include landfill leachate, leaking septic tanks, and municipal storm water runoff (Hiscock et al., 1991; Panno et al., 2008).

Different options to reduce the high nitrate concentration levels in groundwater are available, including improved farming practices, delineation of aquifer protection zones, or dilution with low-nitrate water sources. However, these options are seldom available due to legal, logistic, or economical constraints. Thus, groundwater remediation technologies, such as ion exchange, reverse osmosis, electrodialysis, and Enhanced *in situ* Biodenitrification (EIB) (Haugen et al., 2002), are often the only practical options left to deal with nitrate-contaminated aquifers.

EIB holds environmental and economic advantages over the other remediation methods mentioned, because it is simple, selective, and cost efficient (Smith et al., 2001). The technology is based on the reduction of nitrate to dinitrogen gas by anaerobic heterotrophic facultative bacteria that use nitrate as electron acceptor. Such bacteria are ubiquitous in soil and groundwater (Beauchamp et al., 1989). EIB is feasible anywhere bacteria may thrive, organic electron donors can be supplied, and oxygen levels are below 1-2 mg/L (Korom, 1992). In natural aquifer conditions, a major limiting factor for

biodenitrification is organic matter. Therefore, the main idea behind EIB is the addition of an organic carbon source (acting as electron donor for nitrate reduction and as a carbon source for biomass growth), while controlling a suite of environmental parameters such as the concentrations of other oxidants (e.g. O_2), pH, and nutrient levels (e.g. phosphorous or oligo-elements). Optimal configuration of EIB, involving the presence of one or more injection and extraction wells, is site specific, depending on pumping rate, groundwater flow velocity, and residence time of nitrate in the system (Khan and Spalding, 2004).

The injection of organic carbon during EIB creates a bioactive zone, characterized by the growth of denitrifier biomass, heterogeneously distributed throughout the porous media depending on nutrient availability. Biomass can be found either as suspended matter or as biofilms attached to the solid matrix. Biofilms occur as micro-colonies or aggregates composed by denitrifier microorganisms, extracellular polymeric or proteinic substances (EPS), and potentially trapped dinitrogen gas formed during denitrification (Dupin and McCarty, 2000; Hand et al., 2008; Rittmann, 1993; Vandevivere and Baveye, 1992).

As biofilm develops and the pore space is occupied, partial bioclogging might take place, affecting a number of hydraulic properties. In addition to bioclogging, a reduction of hydraulic conductivity can be associated with the presence of trapped N_2 gas (Amos and Mayer, 2006; Jarsjö and Destouni, 2000). While the word clogging is traditionally defined in terms of the overall reduction in hydraulic conductivity (Vandevivere and Baveye, 1992), the decrease in effective pore volume caused by biofilm growth also changes porosity. Due to the variation of these two hydraulic parameters, changes in groundwater velocity might be recorded (Pavelic et al., 2007; Taylor and Jaffé, 1990; Taylor et al., 1990), changing residence time between injection and extraction wells, thus influencing the

overall capacity for biodenitrification. Furthermore, the spatial heterogeneity of hydraulic properties caused by the inhomogeneous distribution of biofilm throughout the porous media also promotes changes in dispersivity (Seifert and Engesgaard, 2007). Dispersivity is an important parameter as it affects the mixing of nitrate with injected organic substrate, and it is sometimes the limiting factor for the reaction processes (Dentz et al., 2011).

Thus, the amount of biomass and the way it grows significantly affect the performance of EIB facilities. Biomass growth is driven among other things by the feeding strategy, i.e., the frequency of injection, the total carbon supplied, and the resulting carbon-nitrogen ratio (C:N). With the objective of limiting the biomass growth, some authors suggested injecting the electron donor in discrete pulses rather than as a continuous supply (Franzen et al., 1997; Gierczak et al., 2007; Peyton, 1996; Semprini et al., 1991; Semprini et al., 1990; Shouche et al.). Nevertheless, little is known about how the frequency of injection pulses affects biomass growth and nitrate degradation. Regarding the C:N ratio, Vidal-Gavilan et al. (2014) observed that even working with low C:N ratios (C:N=1; below the stoichiometric one: C:N = 2.5), high denitrification rates were achieved after biofilm development. The authors attributed this to the occurrence of endogenous bacterial decay.

Proper understanding of processes occurring during EIB involves the need for multispecies reactive transport modeling (RTM) (Chen and MacQuarrie, 2004; Lee et al., 2006; Rodríguez-Escales et al., 2016). Such models can facilitate exploring a variety of remediation strategies such as injection duration and rate, and concentration of reactants. Nevertheless, there is a need to develop specific models to evaluate how different feeding strategies interact with transport processes.

111 The present work is aimed at developing a model capable of reproducing different
112 feeding injection frequencies (from weekly to daily) with different C:N ratios in a long term
113 column experiment of Enhanced *in situ* Biodenitrification, lasting 342 days (Vidal-Gavilan
114 et al., 2014). This modeling study focusses on the EIB performance in response to the
115 frequency of organic substrate addition as well as the changes in hydraulic and transport
116 properties promoted by the growth of biofilm. Proper understanding of the processes taking
117 place allow defining the optimal injection strategy (frequency and rate) capable of
118 enhancing EIB performance (high performance at low cost) by minimizing the overall
119 supply of labile organic carbon substrate.

120 ## 2 Materials and Methods

121 ### 2.1 Description of the experiment and data set

122 A full description of the experiment is provided in Vidal-Gavilan et al. (2014), and
123 sketched here in Figure 1 for completeness. It consisted of a glass cylindrical column (70
124 cm length, 8 cm inner diameter) filled with unconsolidated sediment from a sandy alluvial
125 aquifer (located in Argentona, NE Spain). The sediment was composed by medium and
126 coarse-grained sand mainly made up of quartz and feldspar and with a small silt content,
127 the organic matter content in the sediment was negligible (Vidal-Gavilan et al., 2014).
128 Water was forced to flow from the bottom to the top of the column with a pump-controlled
129 average flow-rate of 180 mL/d resulting in a residence time in the column of about 6.4
130 days. A total of eight sampling ports were installed: one at the inflow reservoir, six along
131 the column (at 6, 16, 26, 36, 46 and 56 cm from inlet), and one at the outflow, allowing the
132 delineation of aqueous compounds and suspended biomass profiles at different predefined

133 times. The data set provided in Vidal-Gavilan et al. (2014) and used in the modeling effort
134 includes aqueous concentrations of ethanol, nitrate, and biomass at selected times at the
135 sampling ports placed within the column. A control experiment without carbon substrate
136 addition ran for 2 months, and natural denitrification was not observed, as changes in
137 nitrate along the column were lower than 1% (Vidal-Gavilan et al., 2014).

138 The water used in the experiment was obtained from an existing large-diameter well
139 located at the site. Three 25-L containers were used to store the input water for the
140 experiment, filled up at different days (August 2011, December 2011, and April 2012). The
141 well was always purged prior to sampling. No forced deoxygenation took place, so that the
142 input water (see Table 1) was oxic and saturated with oxygen. The experiment ran for 342
143 days at aquifer temperature (15ºC). Ethanol was added as an external organic carbon source
144 by means of four injectors located 16 cm from the inlet (see Figure 1). It was added by
145 mixing it with the input water previous to injection (Table 1). Different feeding strategies
146 were tested during the experiments (Table 2), characterized by different injection
147 frequencies (weekly *versus* daily) and carbon to nitrogen molar ratios (from 2.5 to 1). In
148 this ratio the amount of C is computed from the concentration of ethanol multiplied with
149 the duration of injection (0.5 min). Feeding was twice discontinued, first between days 150
150 and 175 due to pump failure (no water was supplied), and then between days 286 and 311,
151 this time to evaluate the resilience of the system to the absence of feeding (water with no
152 ethanol was supplied during that second period).

153 Two tracer tests were performed, one previous to the start of the experiment, before
154 any feeding took place, and a second one at day 342. The tests were conducted under
155 continuous flow with constant concentration of bromide (1.45 and 2.23 mM, respectively).

During the two tracer tests the flow rate was 835 mL/d. The bromide breakthrough curves were monitored at the outflow point.

2.2 Model construction

Here we describe first the biogeochemical equations used in the biodenitrification model; second, the hydrogeological parameters derived from the two tracer tests; third, the codes used in the modeling effort; and fourth, the calibration process.

2.2.1 EIB biogeochemical model

Biodenitrification was modelled considering both nitrate respiration and biomass growth (see e.g., Rodríguez-Escales et al., 2014). The reactions considered are:

$$r_{ED} = -k_{max} \frac{[ED]}{[ED] + K_{S,ED}} \frac{[EA]}{[EA] + K_{S,EA}} [X] \quad (1)$$

$$r_{EA} = Q r_{ED} - S b [X] \quad (2)$$

$$r_X = -Y_h r_{ED} - b[X] \quad (3)$$

where [ED] is the concentration of the electron donor (ethanol, C_2H_5OH); [EA] that of the electron acceptor (nitrate), and [X] the denitrifier biomass concentration, all expressed in [ML^{-3}]; k_{max} [T^{-1}] is the consumption rate of electron donor per unit value of biomass; $K_{S,ED}$ [ML^{-3}] and $K_{S,EA}$ [ML^{-3}] the half saturation constants of electron donor and acceptor, respectively; b [T^{-1}] a biomass decay constant; Y_h the microbial yield [C biomass / C ethanol], and Q [N nitrate / C ethanol] and S [N nitrate / C endogenous]. Both K_{max} (μ_{max}/Y_h) and K_s were fitting parameters, whereas S and Q were stoichiometric factors

175 determined by the driving denitrification reaction (4). Biomass was conceptualized as
176 having an average chemical composition of $C_5H_7O_2N$ (Porges et al., 1956).

177 $$0.943\ C_2H_5OH + 1\ NO_3^- + 0.489\ H^+ = 0.273\ C_5H_7O_2N + 0.364\ N_2 + 0.511\ HCO_3^- + 1.864\ H_2O \quad (4)$$

178 Equation (4) was determined following the instructions of Rittmann and McCarty (2001)
179 and it applies to the following determined parameter values: (i) the portion of substrate
180 (ethanol) used for cell synthesis during denitrification (Y_h) was 0.724 C-biomass/C-ethanol
181 (in agreement with Rodríguez-Escales et al. 2014); and (ii) the portion of nitrate consumed
182 by substrate oxidation (Q) was 0.53 mol nitrate-mol C-ethanol. The stoichiometric
183 relationship between nitrate and endogenous carbon (S) was 0.92 mol nitrate-mol C
184 endogenous, following (Rodríguez-Escales et al., 2014).

185 Although the injected solution was partly to almost fully oxic (oxygen concentrations
186 measured varied between 0.06 and 0.2 mM), ethanol oxidation by oxygen was and could be
187 neglected. This assumption was based on ethanol consumption by oxygen being between
188 0.1 and 4% of ethanol injected (depending on initial concentrations). Moreover, preliminary
189 models considering instantaneous reduction of oxygen showed that oxygen was consumed
190 within the first 5 cm of the column (results not shown). Considering all of this and in order
191 to simplify the model, ethanol oxidation by oxygen was not contemplated.

192 Nitrite accumulation was not relevant in the experiment (only present during the first
193 20 d, in concentrations below 0.1 mM; whereas nitrate decreased then with 1.2-1.6 mM.).
194 Therefore, the model contemplates only one step reduction from nitrate to dinitrogen gas.
195 The potential accumulation of NO and N_2O was discarded because the system was
196 maintained at low oxygen concentrations, with enough labile organic carbon, and with pH

197 values between 7 and 8; under these conditions complete denitrification is expected (Rivett
198 et al., 2008; Tallec et al., 2008).

199 Most often, the amount of bacteria suspended in the aqueous phase is quite small as
200 compared to that attached to the aquifer matrix (Barry et al., 2002; Rittmann, 1993). As a
201 way to implement a practical model, minimizing the number of fitting parameters, we
202 assumed that all biomass was attached to the solid matrix, and thus immobile, without
203 considering attachment and detachment processes, described for example in Clement et al.
204 (1997). The initial biomass concentration was estimated in 6.5×10^{-8} mmol/kg, considering
205 a most probable number for denitrifying cells equal to 37.5 cel/ml (Vidal-Gavilan et al.
206 2014) and converted to moles using a denitrifier cell weight of 10^{-9} mg (Alvarez et al.,
207 1994). The initial value used in PHT3D was normalized by liter of water.

208 Finally, the column was considered as an open system in equilibrium with the
209 atmosphere because it was open at its upper part. Thus, degassing was allowed if the sum of
210 partial pressures of gases (mainly dinitrogen gas and carbon dioxide) exceeded the
211 atmospheric pressure. Prior to the simulation process, and in order to evaluate the potential
212 hydraulic conductivity variations due to bubble formation, we evaluated the potential
213 building up of denitrification gases. Thus, we ran the model under closed system
214 conditions. The results showed that the hydrostatic pressure was exceeded in most feeding
215 strategies illustrating that degassing could occur. To limit the chance for gas entrapment,
216 which would be the main responsible of changes in hydraulic conductivity (Amos and
217 Mayer, 2006), we purposely ran the column experiment in vertical mode with water
218 flowing upwards. In this way, gas entrapment should have been limited as any gas formed
219 could escape at the top outlet of the column and the flow of gas bubbles and water in the

column were aligned. Furthermore, we expect that the coarse sand (grain size between 1 and 2 mm) used in the column further limited any gas entrapment.

2.2.2 Transport model parameters evaluated from the tracer tests

Two tracer tests with a conservative tracer (Br-) were performed at days 0 and 342 in order to build a conceptual model for conservative transport and to estimate the corresponding hydraulic parameters. Invoking the parsimony principle, we first tried to fit the breakthrough curves with the simplest model, that of the one-dimensional advection-dispersion equation (ADE).

The ADE model could properly reproduce the test performed at time 0, but failed to fit the tail of the experimental BTC obtained during the second test at day 342. As an alternative model we selected a dual porosity model (Delay et al., 2013; Haggerty and Gorelick, 1995; Lawrence et al., 2002; Seifert and Engesgaard, 2007), representing the porous medium as composed of a mobile and of an immobile region that coexist at any given point in the domain. The first one was an aqueous phase where advection and dispersion were the main transport processes, whereas the second one was a (diffusion zone governed by biofilm dynamics). Both regions exchange mass proportionally to the difference in their concentrations at any given time. The equation describing the concentration of species *i* in the mobile zone, $c_{m,i}$, is:

$$\phi_m \frac{\partial C_{m,i}}{\partial t} = -q \frac{\partial C_{m,i}}{\partial x} + \phi_m \frac{D \partial^2 C_{m,i}}{\partial x^2} - \Gamma_i \quad (5)$$

where D is the dispersion coefficient, q is Darcy's velocity, ϕ_m the porosity corresponding to the mobile zone (aqueous phase with aqueous solution), and Γ_i the source-sink term

241 controlling the mass transfer of species i between the mobile (m) and the immobile regions
242 (im) (biofilm phase with microorganisms attached to the sediment), given by:

243 $$\Gamma_i = \alpha \phi_{im} \left(C_{m,i} - C_{im,i} \right) \quad (6)$$

244 with α the mass transfer rate [T^{-1}], ϕ_{im} [-] the porosity associated with the immobile region
245 (volume fraction occupied by the biofilm), and $C_{im,i}$ the concentration of species *i* in the
246 immobile region. The actual total porosity is $\phi_t = \phi_m + \phi_{im}$, and remains constant during
247 biofilm formation. The rationale behind it is that the biofilm colonizes pores that were
248 initially occupied by water in sediments not affected by consolidation or swelling, so that
249 the sediment occupied the same volume at the beginning and end of the experiment. A key
250 parameter characterizing the shape of the BTC in the dual porosity model is the ratio of
251 porosities (Fernàndez-Garcia and Sanchez-Vila, 2015) given by:

252 $$\beta = \frac{\phi_{im}}{\phi_m} = \frac{\phi_t}{\phi_m} - 1 \quad (7)$$

253 **2.2.3 Used codes and calibration process**

254 The PHT3D model code (v. 2.17) (Prommer and Post, 2010) was used to simulate the
255 evolution of groundwater hydrochemistry during enhanced biodenitrification in the column.
256 This model couples the transport simulator MT3DMS (Zheng and Wang, 1999) and the
257 geochemical model PHREEQC-2 (Parkhurst and Appelo, 1999), by means of a sequential
258 split-operator technique. Regarding solute transport, PHT3D incorporates either the
259 traditional ADE, or else the dual domain model through MT3DMS. Since the PHT3D
260 reaction module uses the original PHREEQC-2 database syntax, equilibrium and non-
261 equilibrium reaction chains can be defined. For reactions in equilibrium, the constants were

taken directly from the database. Kinetic reactions such as ethanol degradation and bacterial growth/decay (1-3), not being part of the standard database, were incorporated into the module in the form of BASIC routines, as explained in Rodríguez-Escales et al. (2014) and Carrey et al. (2014).

Regarding the tracer tests, the interpretation using the traditional ADE and the dual domain model was carried out with the CXTFIT code (Toride et al., 1999). We developed the inverse modelling of transport processes using the experimental information of the BTCs from the tracer tests and we determined the following parameters: dispersivity coefficient, total, mobile and immobile porosities, and, dual domain transfer coefficient. Furthermore, CTXFIT provides the confidence interval (95%) of each parameter as well as their corresponding standard deviations. In order to avoid the correlation between immobile porosity and dispersivity coefficient in the transport equation (e.g. Wehrer et al. 2012), the calibration process was divided in two steps. First of all, we calibrated the dispersivity coefficient and the mobile porosity without considering the tail. Then, we incorporated the dual domain model to improve the fittings of the tail, allowing an independent estimation of the immobile porosity. Following this methodology, we only related the dispersivity to the change into the geometry and not also to the diffusion processes avoiding its correlation with immobile porosity.

To assist the biodenitrification model calibration process, the model independent parameter estimation program PEST (Doherty, 2005) was coupled to PHT3D and used to estimate the reaction rate parameters ($k_{max,.}$ $K_{S,ED,}$ $K_{S,EA}$, and b). PEST computed the sensitivities, correlations, and linear uncertainties (confidence intervals) of the optimized model parameters. For the calibration process, the error associated with the measurement

was treated as 95% confidence interval, and weights were applied using the inverse of the standard deviation of this confidence interval (Karlsen et al., 2012). Using this method, values with a higher accuracy get assigned a higher weight and the resulting objective function became dimensionless. Standard ranges for measurement error of chemical sampling were given with an accuracy of 5%. Weights (w) for each chemical species observation i were thus calculated:

$$w_i = \frac{1.96}{\varepsilon_i C_i} \quad (8)$$

where ε is the measurement error described above and C is the observed concentration. For the calibration process, we used the experimental data of nitrate during the first 100 days of the experiment (35 points). The calibration process of the reactive transport was performed by fixing the conservative transport parameters. Finally, we also evaluated the likelihood of the models comparing the Akaike information criterion values (AIC) calculated by PEST.

3 Results and discussion

3.1 Tracer tests interpretation: derivation of transport processes and parameters

The first step is the interpretation of the 1-D conservative tracer tests. The traditional ADE equation was capable of properly fitting the curve corresponding to the first test, but it failed to provide a good fit of the tail of the BTC corresponding to the second test, with a maximum error in estimated concentrations of 3%. On the other hand, the dual domain model was capable to reproduce the tail of the BTC corresponding to the second test indicating a transition from a Fickian description of transport at the start to an anomalous description of transport at the end of the EIB experiment. The reported BTCs are presented

306 in Figure 2, together with the best fits obtained either with code CTXFIT at day 0 (single
307 porosity) and at day 342 (dual porosity); the fitted parameters are listed in Table 3.
308 Groundwater velocity was very similar in the two tests (see Table 3). The hydraulic
309 gradient could not be measured in the applied experimental setup. Therefore, any reduction
310 in hydraulic conductivity due to biofilm growth could not be assessed. Total (single-phase)
311 porosity and dispersivity were estimated from the first test; total porosity, the proportion of
312 immobile and mobile porosity, dispersivity, and the mass transfer rate were estimated from
313 the second one. Total porosity values estimated from both tests were statistically not
314 different, with best estimates of 0.33±0.03 to 0.34±0.05, and estimation intervals largely
315 overlapping (Table 3). However, the dual porosity model estimated an immobile porosity of
316 0.015±0.009 at day 342.

317 There was a remarkable seven-fold increase in the dispersivity coefficient estimated
318 from the two tests, with the mean value changing from 0.48±0.01 to 3.44±0.25 cm (see
319 Table 3). This result is consistent with the observations by Taylor and Jaffé (1990) who
320 also described an increase in immobile porosity linked to an increase in dispersivity in a
321 column experiment colonized by biomass. Several studies also report significant changes in
322 dispersivity, ranging from two- to eight-fold increases, in bioremediation experiments
323 lasting 2-7 weeks (Arnon et al., 2005; Bielefeldt et al., 2002; Hill and Sleep, 2002; Seifert
324 and Engesgaard, 2007; Sharp et al., 1999; Taylor and Jaffé, 1990; Taylor et al., 1990), and
325 as high as a 10-100 fold variation for long duration experiments (Taylor and Jaffé, 1990;
326 Bielefeldt et al., 2002). This increase in dispersivity is generally associated to denitrifier
327 biomass colonizing the sand grains forming the soil skeleton. Thus, while total porosity
328 remained basically constant, a small fraction was colonized by biomass aggregates and

329 micro-colonies, changing its behavior from water accessible by flow (mobile) to
330 inaccessible (immobile). Such aggregates have been reported to induce irregular surfaces of
331 the solid particles (Rittmann, 1993), and consequently, to increase the heterogeneity in the
332 pore size distribution (Seifert and Engesgaard, 2007), thus enhancing dispersivity.

333 The change in the conceptual model of transport was associated with the growth of
334 biofilm during the duration of the experiment. Thus, the fitted parameters of the dual
335 domain model have a clear physical explanation; for example, the calibrated α parameter (α
336 = 0.019±0.018 d^{-1}) can be interpreted as the inverse of the characteristic diffusive time of
337 bromide transport through the immobile phase (thus being equal to 45 days). Moreover, the
338 β value (β = 0.046±0.030) represented the proportion of the void volume occupied by the
339 biofilm (4.65±2.96 %).

340 Regarding the calibration process of the transport parameters, the automatic
341 calibration showed that during the two steps of calibration the parameters were not
342 correlated because the correlation coefficients were lower than 0.95 (Hill et al., 1998).
343 During the first step (calibration using ADE of velocity and dispersion), the correlation
344 among parameters was lower than 0.025 for the two tracer tests. During the second step, the
345 correlation between immobile porosity and the mass transfer coefficient was 0.21. The
346 coefficients of variation (CV) of the parameters of ADE were well estimated, as their
347 values were generally low (less than 0.15). Regarding the parameters of the dual domain
348 model, they were estimated as highly uncertain.

3.2 Long-term modeling of EIB. Impact of organic carbon injection strategies

Based on tracer tests results the column experiment was first interpreted using a Fickian representation of transport, i.e., based on the ADE. Emphasis was placed on the performance of the daily and weekly feeding strategies upon the observed temporal evolution of the concentrations of nitrate, ethanol, and biomass. Since Table 3 displays two dispersivity values corresponding to days 0 and 342, but no intermediate values were obtained, the 342-day column experiment was modeled using both dispersivity values, by assuming that they lasted the full duration of the experiment, thus providing two limiting cases. The column was discretized into 70 elements of 1 cm length. The time discretization was selected to satisfy Peclet and Courant criteria. Dispersive transport was computed by the third-order Total Variation Diminishing solution, a feature available in PHT3D.

The actual data and the fittings with the two dispersivity values are shown in Figure 3. Neither porosity (obtained from the tracer test, 0.33), nor the geochemical parameters of reactions in equilibria (selected from the PHREEQC2 database) were calibrated. The only calibrated parameters were the microbiological ones (Table 4) and, all were in range compared to values reported in the literature. Note that the we compared the μ_{max} parameter instead the k_{max} with literature values, because it only depends on velocity reaction and it is easier to compare. The automatic calibration procedure used for the estimation of kinetic parameters in the denitrification model showed that the evaluated parameters were not cross-correlated, as indicated by their values in the coefficient correlation matrix being below 0.747 (data not shown). That is, given the available observations for model calibration, each model parameter affected the simulated equivalents to the observations sufficiently differently. The values of the coefficients of variation, CVs, were relatively

high, ranging from 0.26 to 0.61. As pointed out by Greskowiak et al. (2005), large CVs do not necessarily imply an incorrect model concept. Instead, it may indicate that the available observation data are insufficient to uniquely constrain (estimate) the parameter, or that there is an underlying physical basis for relatively high CVs.

The lowest dispersivity value (0.48 cm) resulted in a good fitting of the experimental data during the weekly feeding strategy (Figure 3), lasting the first 98 days, indicating that during this period dispersivity did not change significantly. This result is in contrast with other works based on column experiments using somewhat different experimental conditions like organic substrate but were all fed continuously (Bielefeldt et al., 2002; Seifert and Engesgaard, 2007; Taylor and Jaffé, 1990) (Table 5). For example, Seifert and Engesgaard (2007), using acetate and oxygen as electron acceptor, reported an increase in dispersivity from 0.33 cm to 1.1 cm in 64 days. On the other hand, Bielefeldt et al. (2002), in an experiment on propylene glycol degradation using nitrate as electron acceptor, observed a 20-60 fold increase in 15 days in clean sand. Finally, Delay et al. (2013) reported a noticeable change in dispersivity in a 1.4 day column denitrification experiment. In short, from the data in Table 5, it seems that a weekly feeding strategy limits dispersivity increases with time.

We note that Figure 4 reports the modeling results assuming a constant representative dispersivity value all throughout the column. We expect though that most of the biomass colonization took place around the injection point (Kildsgaard and Engesgaard, 2001), associated with the highest EA and ED concentrations and, consequently, the modification of the transport parameters too. Although the general trends were well captured, the

limitation of considering only one set of transport parameters could explain the discrepancies between the experimental data and the simulated results.

During the daily feeding strategy, starting after day 99, the best overall fit of nitrate concentration was obtained with the final dispersivity value of 3.43 cm. This is visible both for time-series (Figure 3) and for spatial profiles (Figure 4). Consequently, the increase in dispersivity seems triggered by the changes in feeding strategy, from weekly to daily pulses. During weekly injection, biomass was not fed homogenously, and probably biomass growth was through colonies or aggregates that did not colonizing the whole sandy media. On the other hand, daily injection drove a more continuous growth of biomass (probably in biofilm form) and favoring the colonization of the whole column (Rittmann, 1993). We thus contend that induced heterogeneity was larger in the daily scenario as compared to the weekly one, and consequently, a seven-fold increase of dispersivity in the former feeding strategy was observed. This increase was smaller than others reported in the literature for continuous feeding (see Table 5 for values and references). This can be explained because the injection was performed in the form of a daily pulse, rather than fully continuous. Besides this change in feeding strategy, the two stop periods in daily feeding strategies could also facilitate the increasing of heterogeneity due to the detachment of biomass and its redistribution through the column (Wehrer et al., 2012). This suggests that both the feeding frequency and the stop periods are key operational parameters that may affect hydraulic parameters and thereby control the transport of chemical species during EIB.

We want to emphasize that the increase of dispersivity was evaluated in a column experiment (1D), thus only considering longitudinal dispersivity. Although it is still unknown how biofilm growth will disturb the dispersivity in 3-D (e.g. field applications),

417 we would expect an increase in the three directions of dispersivity, longitudinal, and
418 transversal both horizontally and vertically. The last two of those having a most significant
419 impact upon the enhancement of spreading and mixing of nutrients (Chiogna et al., 2012;
420 Rolle et al., 2009).

421 The biomass concentration decreased corresponding to the low C:N ratios (Figure 3).
422 Note that the biomass concentration did not differ between feeding strategies I and II,
423 indicating that the injection frequency played a lower role than the C:N ratio. Nevertheless,
424 we hypothesize that the biomass growth was different for each strategy. Whereas during
425 weekly feeding strategy, the biomass distribution should not be continuous, in the daily one
426 we should expect that a connected biofilm was formed. This idea follows the observations
427 of Rittmann (1993), who determined that a continuous feeding causes a biofilm whereas a
428 discontinued one resulted in disconnected biomass aggregates. Although the
429 characterization of the attached biomass could be done at the end of the experiment (e.g.
430 Clement et al. (1997)), we recommend for future research the characterization of the
431 biofilm structure through SEM (Scanning Electron Microscope) images.

432 **3.3 The implication of introducing non-Fickianity in the conceptual model**

433 The incorporation of a dual domain transport model resulted in a slight improvement of the
434 model fit from day 183 onwards (Figure 3 and 4, blue dashed-dotted line). The parameters
435 used in the model are reported in Table 3 for transport processes (last row) and Table 4 for
436 the biogeochemical ones. Note that the mass transfer coefficient had a high standard
437 deviation (0.019) in relation to the parameter value (0.018). Considering that, we run the

model with different mass transfer values. The results showed that the model was not very sensitive to this change (results not shown).

As the fit obtained during the weekly feeding strategy by ADE was quite good, much better than the obtained with the non-Fickian model (Figure 3), we contend that during this period the diffusive transport through the biofilm was negligible. Thus, the conceptualization of the porous medium as a dual domain was not considered until the daily feeding strategy started, that supposed to enhance the biofilm developing (conceptualized as immobile porosity). This improvement in fitting is attributed to modeling the partial transformation of initial pores to non-flowing volume (immobile porosity or diffusive layer) that act as electron donor sink. Yet, it is still unknown at which point of the experiment this process was relevant. This could only be assessed by the incorporation of non-invasive techniques to monitor biofilm evolution in future studies. We emphasize that water velocity conditioned the significance of involving a dual domain into the conceptual transport model. Thus, the impact of a dual domain model in the tracer test interpretation (Figure 2) was more significant than that on the biodenitrification experiment (Figure 3-4) because the water velocity was higher (0.5 m/d instead of 0.1 m/d) and thus the time available for mass transfer between the domain was less. Although this difference in velocity, we want to remark that the dual domain model was more likely than the ADE model because its AIC value was the lowest one (203.22 compared to 212.55).

3.4 Significance of the C:N ratio and implications for EIB design

In the scenarios with the lowest C:N ratios (strategies III, days 206-252 and IV, days 253-342), the model correctly reproduces the experimental data of nitrate and ethanol being

completely consumed inside the column (not detected at the outlet). This means that the source of organic carbon was used optimally, fully consumed, as opposed to that observed in strategy I. Note that the increase in dispersivity resulted in enhanced spreading and then mixing of the injected ethanol with nitrate, enabling a more efficient substrate use.

Another parameter that helped defining the success of the different injection strategies is the stress produced upon the biomass population. When the carbon load was reduced (strategies III and IV), the modeled biomass diminished (see Figure 3). However, nitrate remained undetected, indicating that denitrification was partially linked to biomass decay (endogenous respiration) meaning that there was not enough external carbon to maintain the large biomass population (see Figure 5). The use of endogenic carbon as electron donor in bioremediation facilities has already been reported in other works (Béranger et al., 2006; Rodríguez-Escales et al., 2016). The decrease in biomass concentration indicated that the low C:N strategies were not sustainable in time. Nevertheless, working with low C:N could be a good tool to reduce the risk of clogging.

Besides this, the amount of ethanol used in these strategies was lower than in strategies I and II (Figure 6), which would imply important savings (the main cost in an EIB operation is electron donor injection). A proper design of the amount of carbon supplied could represent significant savings in an EIB technology. For these reasons, we recommend applying low C:N strategies when the system has reached maturity (complete denitrification achieved, mature biofilm, no nitrite accumulation) and/or when an important risk of clogging exists (monitored with continuous or semi continuous measurement of hydraulic conductivity and mobile porosity).

4 Summary and conclusions

An Enhanced *In situ* Biodenitrification experiment, performed in a 70 cm long column under virtually constant flow rate and different feeding strategies was modeled. Injection strategies were defined in terms of periodicity of injection of organic carbon (ethanol), and thus resulting C:N ratio. A long term reactive transport (342 d) model based on the Advection Dispersion Equation (ADE) fitted properly most of the experimental data.

Throughout the experiment, estimated dispersivity varied from the beginning to the end of the experiment. During the weekly supply strategy I (first 98 days), the best fit was obtained using a low dispersivity value (0.48 cm), whereas during the daily strategy, it was best fitted with a larger dispersivity value (3.43 cm). We attributed this increase to the change in injection periodicity, from weekly to daily, after day 98, resulting in biofilm growth. Furthermore, after day 252, with a very mature system, data fitted better using a dual-domain model (i.e., non-Fickian) as compared to one based on the ADE. This change was associated with the presence of a diffusive layer (biofilm) increasing its relevance with time. Although the dynamic conditions of the system, the presented model has been capable of reproducing satisfactorily the experimental observations in all feeding strategies.

On the other hand, reducing the C:N ratio below the stoichiometric requirements allowed the optimization of ethanol injection into the system avoiding its presence at the column outlet. At this point, biomass decay increased and the endogenous carbon acted as partial source of electron donor during the denitrification process. Nevertheless, the decrease of modelled biomass concentration in time showed that this strategy is not

503 sustainable at long term and that it only can be used when a mature biofilm exists in the
504 subsurface.

505 Our work has shown that besides other parameters (nutrient loading, flow rate, or grain
506 size), injection frequency is a significant operational parameter that can affect a number of
507 hydraulic parameters, notably dispersivity. This finding could be extended to promote field
508 Enhanced *In Situ* Biodenitrification (EIB) applications. A larger dispersivity value offers
509 the possibility of enhancing spreading of injected solutes, increasing the area treated per
510 injection point and limiting the organic carbon loss in this particular *in situ* technique. Thus,
511 this will promote the growth of biofilm and, when a mature system is eventually reached,
512 reducing the C:N ratio can minimize the risk of clogging. So, in order to improve efficiency
513 and saving costs in real field scale applications, feeding strategy in terms of frequency and
514 C:N relationship should be evaluated before the design and construction of EIB
515 installations, as well as during its operation.

516 **Acknowledgements**

517 We thank the three reviewers and the associate editor for their comments and
518 suggestions, which helped improve the quality of the manuscript. This work was financed
519 by projects CGL2011-29975-C04-01/04, and CSD2009-00065 Consolider-SCARCE
520 project from the Spanish Government, as well as projects 2014-SGR-1377 and TEM-2009
521 from the Catalan Government, and MARSOL FP7-ENV-2013-WATER-INNO-DEMO
522 from the EU. XS acknowledges support from the ICREA Academia Program.

523

References

Alvarez, P., Anid, P., Vogel, T., 1994. Kinetics of Toluene Degradation by Denitrifying Aquifer Microorganisms. J. Environ. Eng., 120(5): 1327-1336. DOI:10.1061/(ASCE)0733-9372(1994)120:5(1327)

Amos, R.T., Mayer, K.U., 2006. Investigating the role of gas bubble formation and entrapment in contaminated aquifers: Reactive transport modelling. J. Contam. Hydrol., 87(1–2): 123-154. DOI:http://dx.doi.org/10.1016/j.jconhyd.2006.04.008

Arnon, S., Adar, E., Ronen, Z., Yakirevich, A., Nativ, R., 2005. Impact of microbial activity on the hydraulic properties of fractured chalk. J. Contam. Hydrol., 76(3-4): 315-36. DOI:10.1016/j.jconhyd.2004.11.004

Barry, D.A. et al., 2002. Modelling the fate of oxidisable organic contaminants in groundwater. Adv. Water Resour., 25(8–12): 945-983. DOI:10.1016/S0309-1708(02)00044-1

Beauchamp, E.G., Trevors, J.T., Paul, J.W., 1989. Carbon Sources for Bacterial Denitrification. In: Stewart, B.A. (Ed.), Adv. Soil. Sci. Springer New York, pp. 113-142. DOI:10.1007/978-1-4613-8847-0_3

Bielefeldt, A., McEachern, C., Illangasekare, T., 2002. Hydrodynamic Changes in Sand due to Biogrowth on Naphthalene and Decane. J. Environ. Eng., 128(1): 51-59. DOI:10.1061/(ASCE)0733-9372(2002)128:1(51)

Béranger, S., Sleep, B., Sherwood Lollar, B., Brown, A., 2006. Isotopic Fractionation of Tetrachloroethene Undergoing Biodegradation Supported by Endogenous Decay. J. Environ. Eng., 132(7): 725-735. DOI:10.1061/(ASCE)0733-9372(2006)132:7(725)

Böhlke, J.-K., 2002. Groundwater recharge and agricultural contamination. Hydrogeol. J., 10(1): 153-179. DOI:10.1007/s10040-001-0183-3

547 Carrey, R. et al., 2014. Nitrate attenuation potential of hypersaline lake sediments in central Spain:
548 Flow-through and batch experiments. J. Contam. Hydrol., 164(0): 323-337.
549 DOI:http://dx.doi.org/10.1016/j.jconhyd.2014.06.017
550 Chen, D.J.Z., MacQuarrie, K.T.B., 2004. Numerical simulation of organic carbon, nitrate, and
551 nitrogen isotope behavior during denitrification in a riparian zone. J. Hydrol., 293(1–4):
552 235-254. DOI:10.1016/j.jhydrol.2004.02.002
553 Chiogna, G., Hochstetler, D.L., Bellin, A., Kitanidis, P.K., Rolle, M., 2012. Mixing, entropy and
554 reactive solute transport. Geophysical Research Letters, 39(20): L20405.
555 DOI:10.1029/2012GL053295
556 Clement, T.P., Peyton, B.M., Skeen, R.S., Jennings, D.A., Petersen, J.N., 1997. Microbial growth
557 and transport in porous media under denitrification conditions: experiments and
558 simulations. J. Contam. Hydrol., 24(3–4): 269-285. DOI:http://dx.doi.org/10.1016/S0169-
559 7722(96)00014-9
560 Delay, F., Porel, G., Chatelier, M., 2013. A dual flowing continuum approach to model
561 denitrification experiments in porous media colonized by biofilms. J. Contam. Hydrol.,
562 150(0): 12-24. DOI:http://dx.doi.org/10.1016/j.jconhyd.2013.04.001
563 Dentz, M., Le Borgne, T., Englert, A., Bijeljic, B., 2011. Mixing, spreading and reaction in
564 heterogeneous media: A brief review. J. Contam. Hydrol., 120–121(0): 1-17.
565 DOI:http://dx.doi.org/10.1016/j.jconhyd.2010.05.002
566 Doherty, J., 2005. PEST: model independent parameter estimation. Watermark Numerical
567 Computing, fifth edition of user manual.
568 Dupin, H.J., McCarty, P.L., 2000. Impact of Colony Morphologies and Disinfection on Biological
569 Clogging in Porous Media. Environ. Sci. Technol., 34(8): 1513-1520.
570 DOI:10.1021/es990452f
571 European Environment Agency, E., 2007. Present concentration of nitrate in groundwater bodies in
572 European countries, 2003.

573 Fernàndez-Garcia, D., Sanchez-Vila, X., 2015. Mathematical equivalence between time-dependent
574 single-rate and multirate mass transfer models. Water Resour. Res., 51(5): 3166-3180.
575 DOI:10.1002/2014WR016348
576 Franzen, M.E.L., Petersen, J.N., Clement, T.P., Hooker, B.S., Skeen, R.S., 1997. Pulsing of
577 multiple nutrients as a strategy to achieve large biologically active zones during in situ
578 carbon tetrachloride remediation. Comput. Geosci., 1(3): 271-288.
579 DOI:10.1023/A:1011573429996
580 Gierczak, R., Devlin, J.F., Rudolph, D.L., 2007. Field test of a cross-injection scheme for
581 stimulating in situ denitrification near a municipal water supply well. J. Contam. Hydrol.,
582 89(1–2): 48-70. DOI:http://dx.doi.org/10.1016/j.jconhyd.2006.08.001
583 Greskowiak, J., Prommer, H., Vanderzalm, J., Pavelic, P., Dillon, P., 2005. Modeling of carbon
584 cycling and biogeochemical changes during injection and recovery of reclaimed water at
585 Bolivar, South Australia. Water Resour. Res., 41(10): W10418.
586 DOI:10.1029/2005WR004095
587 Haggerty, R., Gorelick, S., 1995. Multiple-Rate Mass Transfer for Modeling Diffusion and Surface
588 Reactions in Media with Pore-Scale Heterogeneity. Water Resour. Res., 31(10): 2383-2400.
589 DOI:10.1029/95WR10583
590 Hand, V.L., Lloyd, J.R., Vaughan, D.J., Wilkins, M.J., Boult, S., 2008. Experimental studies of the
591 influence of grain size, oxygen availability and organic carbon availability on bioclogging
592 in porous media. Environ. Sci. Technol., 42(5): 1485-91.
593 Haugen, K.S., Semmens, M.J., Novak, P.J., 2002. A novel in situ technology for the treatment of
594 nitrate contaminated groundwater. Water Res., 36(14): 3497-3506.
595 DOI:http://dx.doi.org/10.1016/S0043-1354(02)00043-X
596 Hill, D.D., Sleep, B.E., 2002. Effects of biofilm growth on flow and transport through a glass
597 parallel plate fracture. J. Contam. Hydrol., 56(3-4): 227-46.

598 Hill, M.C., Cooley, R.L., Pollock, D.W., 1998. A Controlled Experiment in Ground Water Flow
599 Model Calibration. Ground Water, 36(3): 520-535. DOI:10.1111/j.1745-
600 6584.1998.tb02824.x
601 Hiscock, K.M., Lloyd, J.W., Lerner, D.N., 1991. Review of natural and artificial denitrification of
602 groundwater. Water Res., 25(9): 1099-1111. DOI:http://dx.doi.org/10.1016/0043-
603 1354(91)90203-3
604 Jahangir, M.M.R., Johnston, P., Khalil, M.I., Richards, K.G., 2012. Linking hydrogeochemistry to
605 nitrate abundance in groundwater in agricultural settings in Ireland. J. Hydrol., 448–449:
606 212-222. DOI:http://dx.doi.org/10.1016/j.jhydrol.2012.04.054
607 Jarsjö, J., Destouni, G., 2000. Degassing of deep groundwater in fractured rock around boreholes
608 and drifts. Water Resour. Res., 36(9): 2477-2492. DOI:10.1029/2000WR900131
609 Karlsen, R.H., Smits, F.J.C., Stuyfzand, P.J., Olsthoorn, T.N., van Breukelen, B.M., 2012. A post
610 audit and inverse modeling in reactive transport: 50 years of artificial recharge in the
611 Amsterdam water supply dunes. J. Hydrol., 454–455(0): 7-25.
612 DOI:http://dx.doi.org/10.1016/j.jhydrol.2012.05.019
613 Khan, I.A., Spalding, R.F., 2004. Enhanced in situ denitrification for a municipal well. Water Res.,
614 38(14–15): 3382-3388. DOI:http://dx.doi.org/10.1016/j.watres.2004.04.052
615 Kildsgaard, J., Engesgaard, P., 2001. Numerical analysis of biological clogging in two-dimensional
616 sand box experiments. J. Contam. Hydrol., 50(3–4): 261-285.
617 DOI:http://dx.doi.org/10.1016/S0169-7722(01)00109-7
618 Korom, S.F., 1992. Natural denitrification in the saturated zone: A review. Water Resour. Res.,
619 98(6). DOI:doi:10.1029/92WR00252
620 Lawrence, A.E., Sanchez-Vila, X., Rubin, Y., 2002. Conditional moments of the breakthrough
621 curves of kinetically sorbing solute in heterogeneous porous media using multirate mass
622 transfer models for sorption and desorption. Water Resour. Res., 38(11): 1248.
623 DOI:10.1029/2001WR001006

624 Lee, M.-S., Lee, K.-K., Hyun, Y., Clement, T.P., Hamilton, D., 2006. Nitrogen transformation and
625 transport modeling in groundwater aquifers. Ecol. Modell., 192(1–2): 143-159.
626 DOI:10.1016/j.ecolmodel.2005.07.013
627 Organisation for Economic Co-operation and Development, O., 2008. Environmental performance
628 of agriculture in OECD countries since 1990.
629 Panno, S.V., Kelly, W.R., Hackley, K.C., Hwang, H.-H., Martinsek, A.T., 2008. Sources and fate of
630 nitrate in the Illinois River Basin, Illinois. J. Hydrol., 359(1–2): 174-188.
631 DOI:http://dx.doi.org/10.1016/j.jhydrol.2008.06.027
632 Parkhurst, D.L., Appelo, C.A.J., 1999. User's guide to PHREEQC (version 2) - a computer program
633 for speciation, reaction-path, 1D-transport, and inverse geochemical calculations., U.S.
634 GEOLOGICAL SURVEY.
635 Pavelic, P. et al., 2007. Water quality effects on clogging rates during reclaimed water ASR in a
636 carbonate aquifer. J. Hydrol., 334(1–2): 1-16.
637 DOI:http://dx.doi.org/10.1016/j.jhydrol.2006.08.009
638 Peyton, B.M., 1996. Improved biomass distribution using pulsed injections of electron donor and
639 acceptor. Water Res., 30(3): 756-758. DOI:http://dx.doi.org/10.1016/0043-1354(95)00220-
640 0
641 Porges, N., Jasewicz, L., Hoover, S., 1956. Principles of biological oxidation. In biological
642 treatment of sewage and industrial wastes. Reinhold. Publ., New York.
643 Prommer, H., Post, V., 2010. A Reactive Multicomponent Transport Model for Saturated Porous
644 Media. User's Manual. v2.10.
645 Rittmann, B.E., 1993. The significance of biofilms in porous media. Water Resour. Res., 29(7):
646 2195-2202. DOI:10.1029/93WR00611
647 Rittmann, B.E., McCarty, P.L., 2001. Environmental biotechnology : principles and applications.
648 McGraw-Hill, cop. 2001.

649 Rivett, M.O., Buss, S.R., Morgan, P., Smith, J.W.N., Bemment, C.D., 2008. Nitrate attenuation in
650 groundwater: A review of biogeochemical controlling processes. Water Res., 42(16): 4215-
651 4232. DOI:10.1016/j.watres.2008.07.020
652 Rodríguez-Escales, P., Folch, A., Vidal-Gavilan, G., van Breukelen, B.M., 2016. Modeling
653 biogeochemical processes and isotope fractionation of enhanced in situ biodenitrification in
654 a fractured aquifer. Chem. Geol., 425: 52-64.
655 DOI:http://dx.doi.org/10.1016/j.chemgeo.2016.01.019
656 Rodríguez-Escales, P., van Breukelen, B., Vidal-Gavilan, G., Soler, A., Folch, A., 2014. Integrated
657 modeling of biogeochemical reactions and associated isotope fractionations at batch scale:
658 A tool to monitor enhanced biodenitrification applications. Chem. Geol., 365(0): 20-29.
659 DOI:http://dx.doi.org/10.1016/j.chemgeo.2013.12.003
660 Rolle, M., Eberhardt, C., Chiogna, G., Cirpka, O.A., Grathwohl, P., 2009. Enhancement of dilution
661 and transverse reactive mixing in porous media: Experiments and model-based
662 interpretation. J. Contam. Hydrol., 110(3–4): 130-142.
663 DOI:http://dx.doi.org/10.1016/j.jconhyd.2009.10.003
664 Seifert, D., Engesgaard, P., 2007. Use of tracer tests to investigate changes in flow and transport
665 properties due to bioclogging of porous media. J. Contam. Hydrol., 93(1–4): 58-71.
666 DOI:http://dx.doi.org/10.1016/j.jconhyd.2007.01.014
667 Semprini, L. et al., 1991. In-situ biotransformation of carbon tetrachloride under anoxic conditions.
668 Semprini, L., Roberts, P.V., Hopkins, G.D., McCarty, P.L., 1990. A Field Evaluation of In-Situ
669 Biodegradation of Chlorinated Ethenes: Part 2, Results of Biostimulation and
670 Biotransformation Experiments. Ground Water, 28(5): 715-727. DOI:10.1111/j.1745-
671 6584.1990.tb01987.x
672 Sharp, R.R., Cunningham, A.B., Komlos, J., Billmayer, J., 1999. Observation of thick biofilm
673 accumulation and structure in porous media and corresponding hydrodynamic and mass

674 transfer effects. Water Sci. Technol., 39(7): 195-201. DOI:http://dx.doi.org/10.1016/S0273-
675 1223(99)00168-7
676 Shouche, M.J., Petersen, J.N., Skeen, R.S., Use of a mathematical model for prediction of optimum
677 feeding strategies forin situ bioremediation. Appl. Biochem. Biotech., 39(1): 763-779.
678 DOI:10.1007/BF02919034
679 Smith, R.L., Miller, D.N., Brooks, M.H., Widdowson, M.A., Killingstad, M.W., 2001. In situ
680 stimulation of groundwater denitrification with formate to remediate. Environ. Sci.
681 Technol., 35(1): 196-203.
682 Tallec, G., Garnier, J., Billen, G., Gousailles, M., 2008. Nitrous oxide emissions from denitrifying
683 activated sludge of urban wastewater treatment plants, under anoxia and low oxygenation.
684 Bioresource Technology, 99(7): 2200-2209.
685 DOI:http://dx.doi.org/10.1016/j.biortech.2007.05.025
686 Taylor, S.W., Jaffé, P.R., 1990. Biofilm growth and the related changes in the physical properties of
687 a porous medium: 3. Dispersivity and model verification. Water Resour. Res., 26(9): 2171-
688 2180. DOI:10.1029/WR026i009p02171
689 Taylor, S.W., Milly, P.C.D., Jaffé, P.R., 1990. Biofilm growth and the related changes in the
690 physical properties of a porous medium: 2. Permeability. Water Resour. Res., 26(9): 2161-
691 2169. DOI:10.1029/WR026i009p02161
692 Toride, N., Leij, F.J., van Genuchten, M.T., 1999. The CXTFIT code for estimating transport
693 parameters from laboratory or field tracer experiments.
694 Vandevivere, P., Baveye, P., 1992. Saturated Hydraulic Conductivity Reduction Caused by Aerobic
695 Bacteria in Sand Columns. Soil Sci. Soc. Am. J.(1): 1-13.
696 Vidal-Gavilan, G., Carrey, R., Solanas, A., Soler, A., 2014. Feeding strategies for groundwater
697 enhanced biodenitrification in an alluvial aquifer: Chemical, microbial and isotope
698 assessment of a 1D flow-through experiment. Sci.Total Environ., 494–495(0): 241-251.
699 DOI:http://dx.doi.org/10.1016/j.scitotenv.2014.06.100

Wehrer, M., Jaesche, P., Totsche, K.U., 2012. Modeling the kinetics of microbial degradation of deicing chemicals in porous media under flow conditions. Environ. Pollut., 168: 96-106. DOI:http://dx.doi.org/10.1016/j.envpol.2012.04.016

Zheng, C., Wang, P.P., 1999. MT3DMS: A modular three-dimensional multispecies model for simulation of advection, dispersion and chemical reactions of contaminants in groundwater systems. Documentation and User's Guide, Contract Reo. SERDP-99-41. U.S. Army Eng. Res. and Dev. Cent., Vicksburg, Miss.

Figure captions

Figure 1. Experimental flow-through system and location of the sampling ports.

Figure 2. Model fits using the ADE (black lines) and a dual domain model (red dashed lines). Square symbols (□) correspond to measurements corresponding to the tracer test performed at day 0 (red and black lines run in top of each other), whereas circles (○) correspond to the BTC from the test at day 342. The error bars are related to the bromide analyses.

Figure 3. Results of the EIB models considering different injection strategies at the outflow of the column (70 cm). The black and the red solid lines were obtained with dispersivity values of 0.48 and 3.43 cm, respectively, considering an ADE equation. The dashed-dotted blue line corresponds to a model using a dispersivity value of 3.43 cm and a dual model mass transfer. The dashed black line corresponds to ethanol concentration in the injection solution. Grey areas represents the two periods without feeding. The bottom plot shows the simulated biomass concentrations (represented in mM) at the last cell of the model domain (70 cm).

Figure 4. Nitrate distance profiles (simulated vs. measured) at 12 different times. In each plot, the first number represents the sampling day, and that in brackets reflects the elapsed time since the last injection period. The black and the red dashed lines were obtained with dispersivity values of 0.48 and 3.43 cm, respectively, considering an ADE equation. The blue dashed doted line in the last two plots corresponds to a model using a dispersivity value of 3.43 cm and a dual model mass transfer. The grey zone corresponds to the injection point.

Figure 5. Detail of feeding strategies with low C:N ratio without considering decay of biomass (top line) and biomass decay (bottom line). Filling zone indicates the importance of biomass decay on nitrate consumption rates under low C:N.

Figure 6. Comparison of the amount of ethanol used in injections and percentage of denitrification achieved by the different feeding strategies. The percentage of denitrification was calculated as the difference in nitrate mass between the inlet and the outlet of the column divided by the nitrate mass at the inlet.

Table captions

Table 1. Average concentration of different species in the input water. Nitrate concentration (*) varied during the experiment due to seasonal nitrate oscillations within the aquifer.

Table 2. Summary of the different feeding strategies (I to IV) tested during the experiment, in terms of feeding frequency, ethanol concentration supplied, ratio of C (external organic carbon source concentration) to N (nitrate concentration), and duration.

Table 3. Hydraulic parameters estimated for the two bromide tracer tests. The standard deviation was calculated by using the inverse problem with CTXFIT. The interpretation models were different for the two tests: the initial one (day 0) with an ADE model; the second one (day 342) with the dual domain model, thus involving two additional parameters. The R^2 of two fitted curves were 0.999 and 0.998, respectively.

749 **Table 4.** Biogeochemical constants used in the denitrification model, compared with values
750 compiled from the literature. Both the median and the standard deviation were determined
751 by automatic calibration using PEST.

752 **Table 5.** Comparison between the values obtained in this work and in similar experiments
753 compiled from the literature, including feeding strategies, organic carbon inflow, flow rate
754 and estimated increase in the dispersivity after some period of time.

Figure1

Click here to download high resolution image

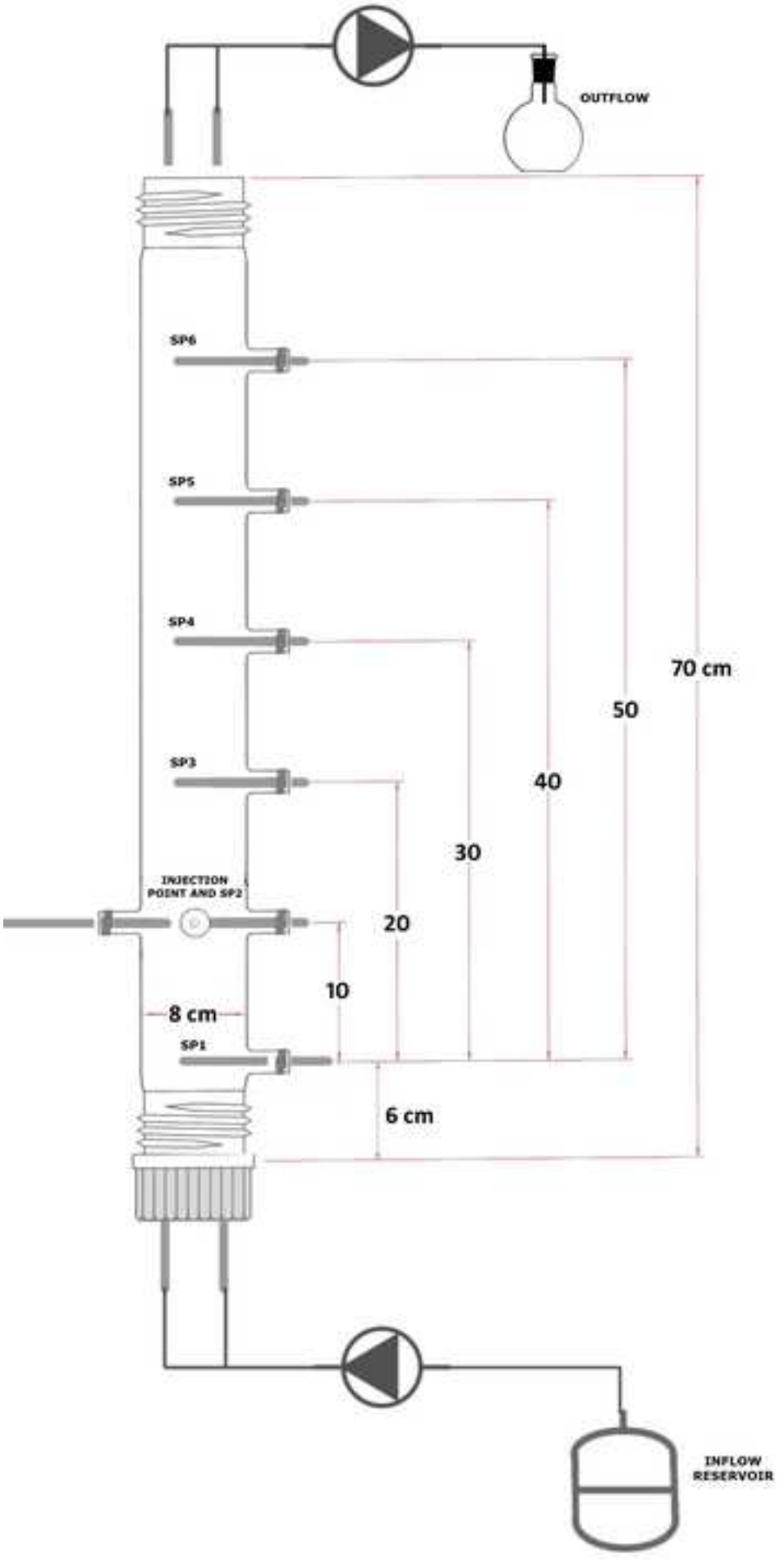

Figure2

Click here to download high resolution image

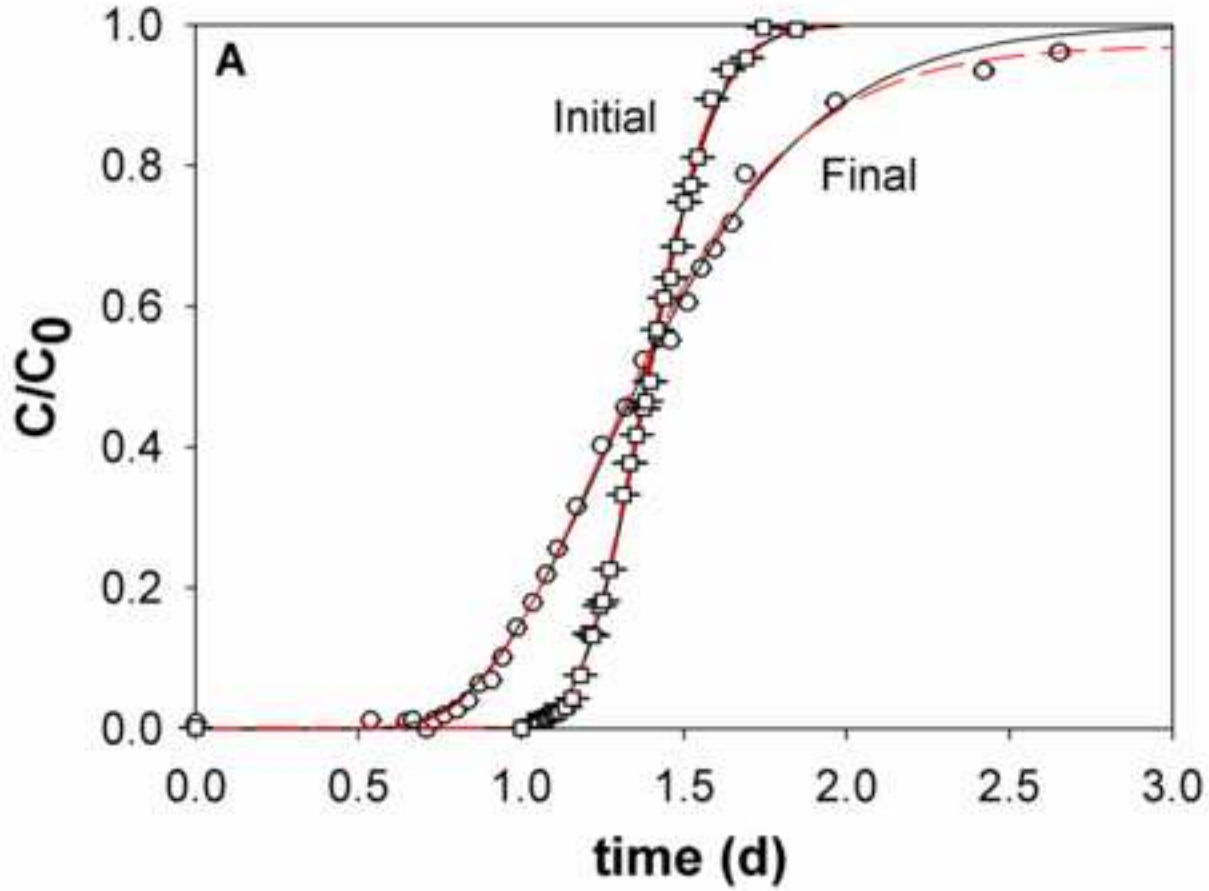

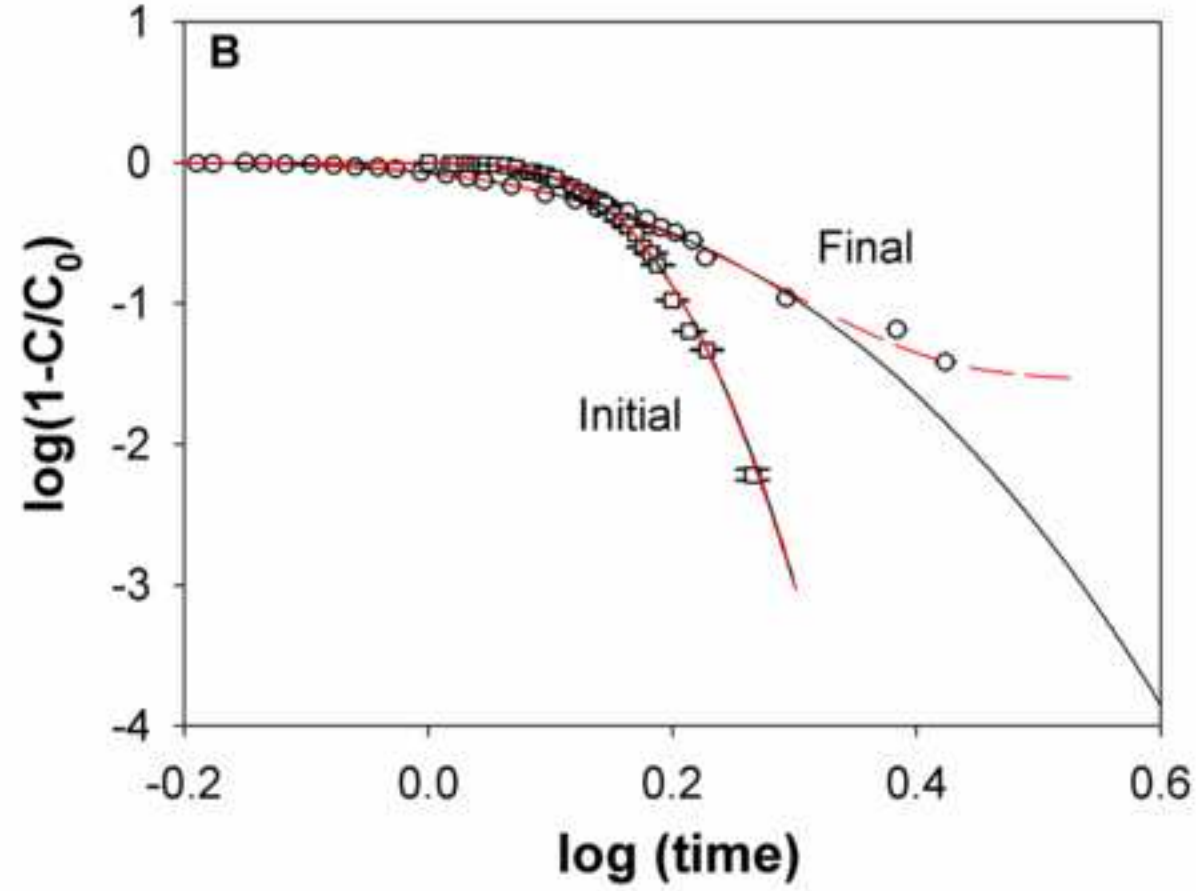

Figure3

Click here to download high resolution image

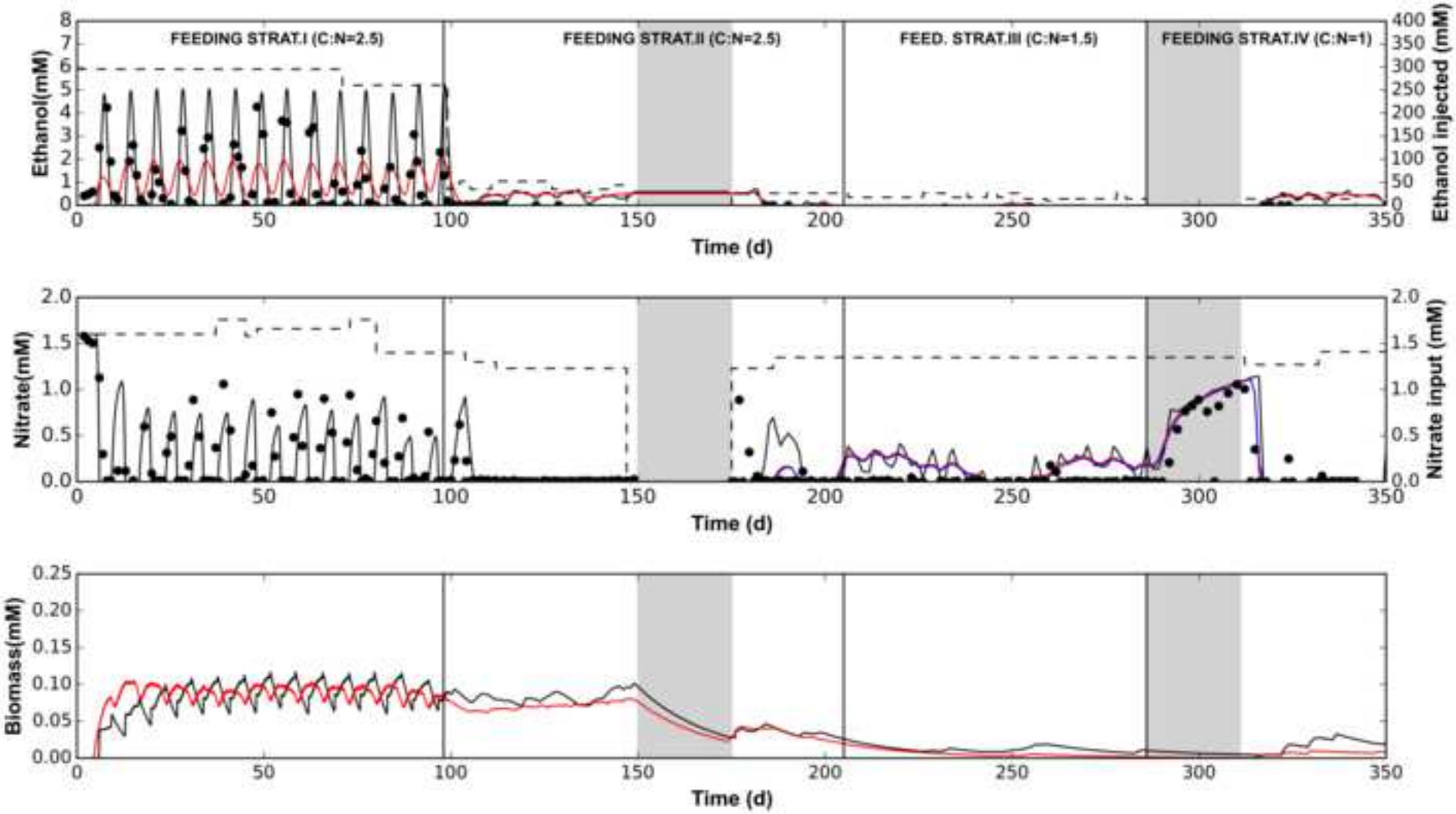

Figure4

Click here to download high resolution image

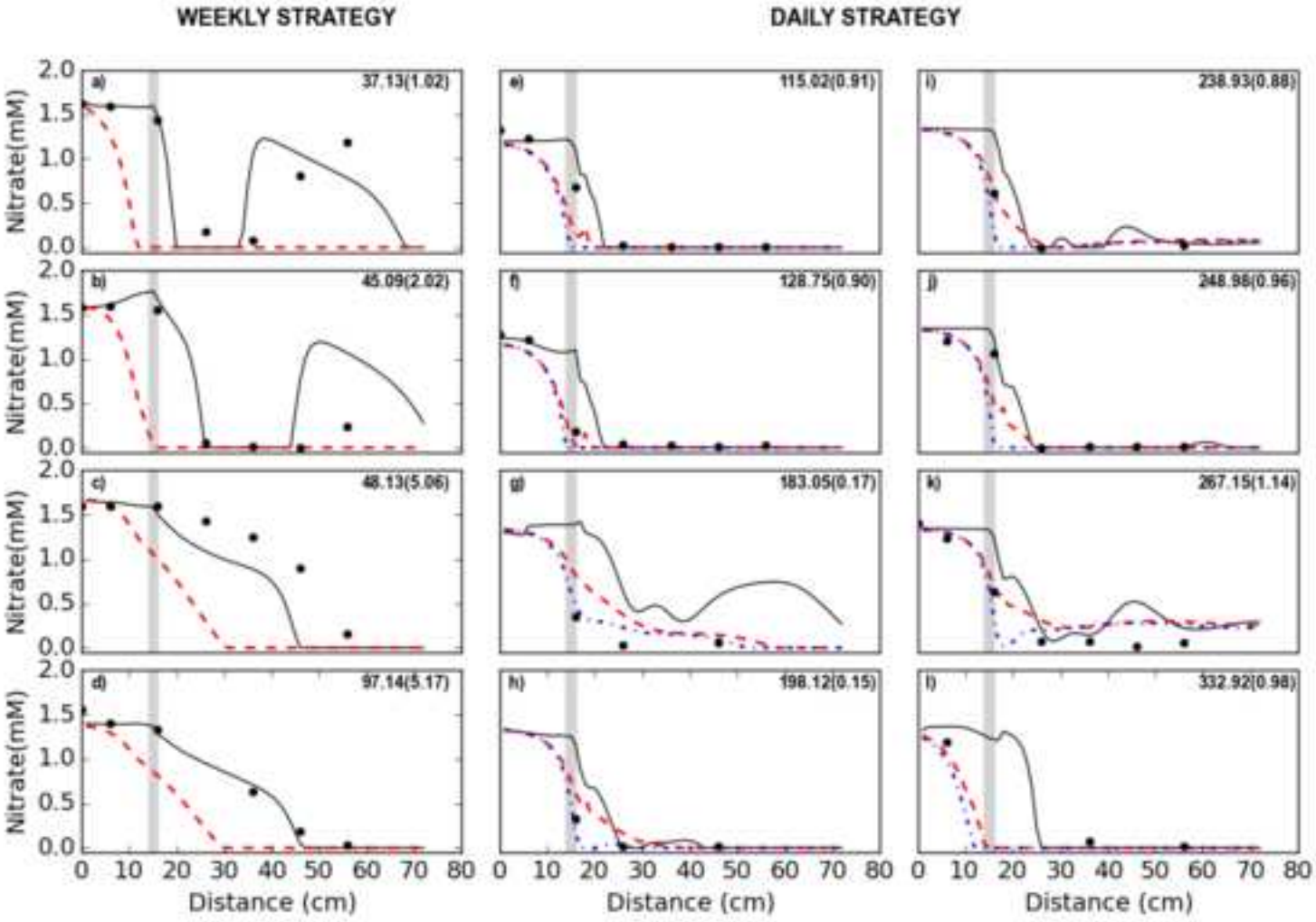

Figure5

Click here to download high resolution image

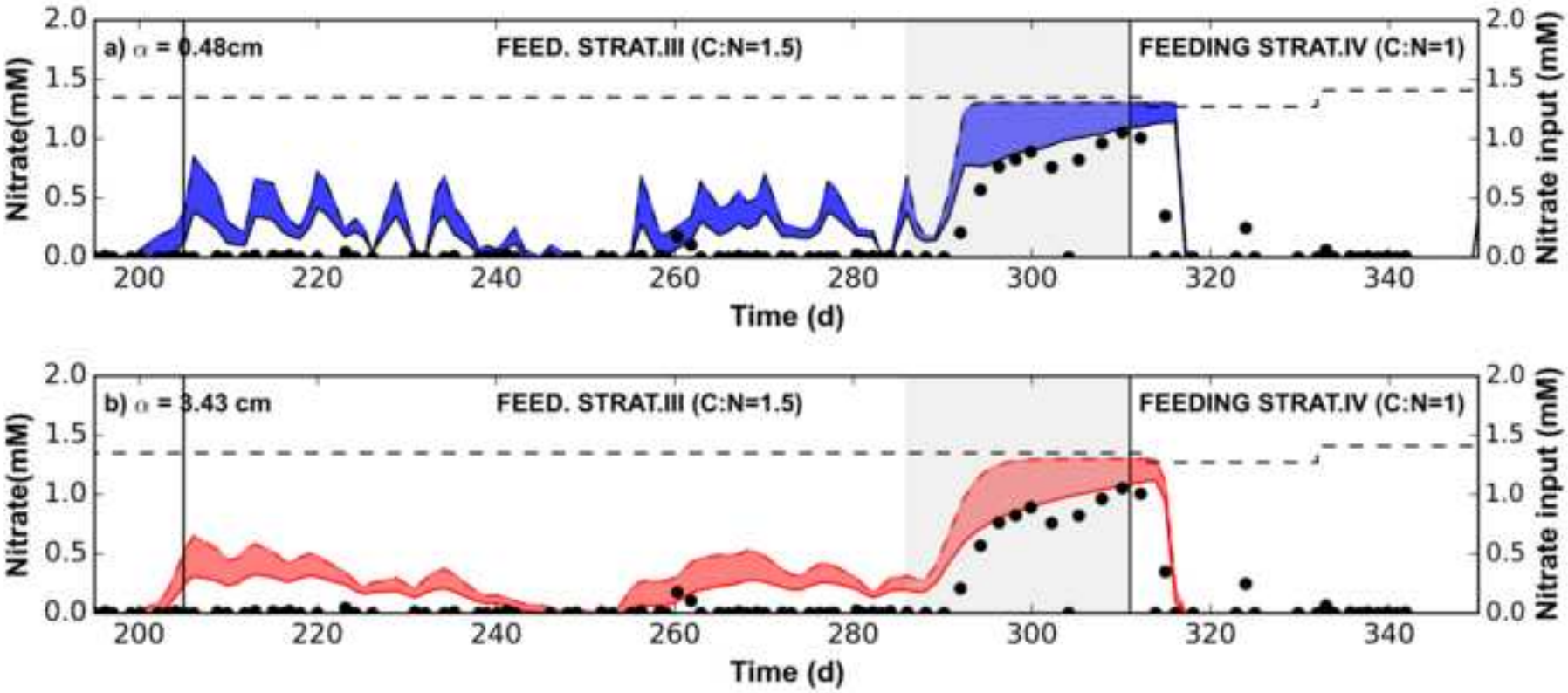

Figure6

Click here to download high resolution image

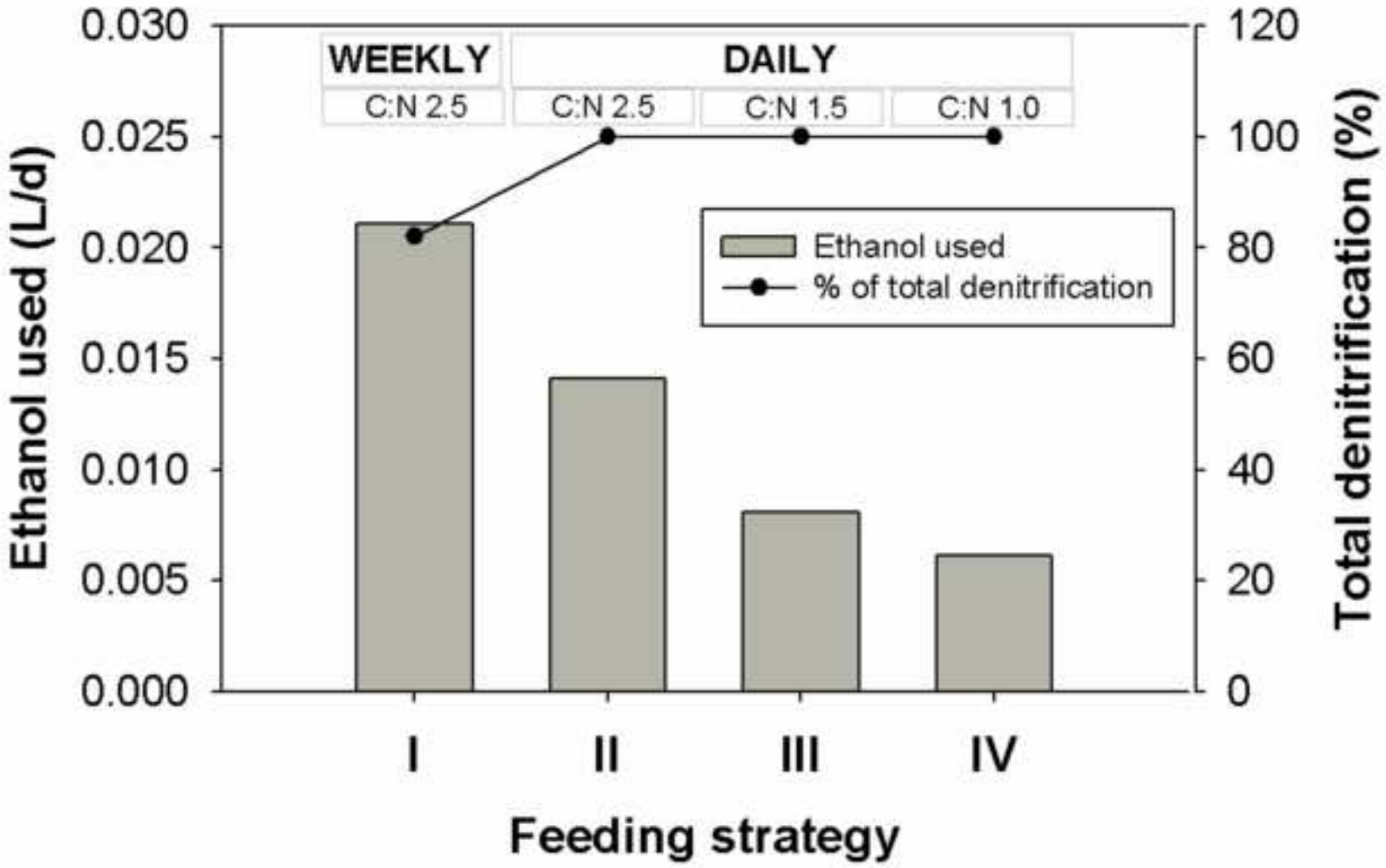

Table1

Click here to download Table: Table1_v2.docx

Parameter	Unit	Column solution	Injected solution
pH		7.2 ± 0.1	7.2 ± 0.1
Temperature	ºC	15	15
Nitrate	mM	1.2-1.6 (*)	1.2-1.6 (*)
DIC	mM	7.2 ± 1.0	7.2 ± 1.0
Chloride	mM	0.10 ± 0.04	0.10 ± 0.04
Sulfate	mM	1.2 ± 0.1	1.2 ± 0.1
Calcium	mM	3.40 ± 0.07	3.40 ± 0.07
Sodium	mM	2.20 ±0.04	2.20 ±0.04
Magnesium	mM	1.60 ±0.03	1.60 ±0.03
Potassium	mM	0.100 ±0.001	0.100 ±0.001
Ethanol	mM	-	14-292
Biomass	mM	2.3×10^{-7}	

Table2

Click here to download Table: Table2_v2.docx

Feeding strategy	Feeding frequency	Average C:N	Ethanol injected (mM ethanol)	Days of experiment
I	Weekly	2.5	261-292	1-98
II	Daily	2.5	26-35	99-205*
III	Daily	1.5	17	206-287
IV	Daily	1	14	287-342**

*Supply of water was discontinued between days 150 and 175

**Supply of organic carbon was discontinued between days 286 and 311

Table3

Click here to download Table: Table3_v2.docx

	Groundwater velocity ($m\ d^{-1}$)	MODEL TYPE	Mobile Porosity	Dispersivity (cm)	Mass transfer parameter (α, d^{-1})	Immobile porosity
Initial	0.5036 ± 0.0004	ADE	0.331 ± 0.033	0.485 ± 0.006	N/A	N/A
End	0.5107 ± 0.0018	Dual domain	0.326 ± 0.044	3.440 ± 0.246	0.019± 0.018	0.015 ± 0.009

Table4

Click here to download Table: Table4_v2.docx

Parameter	Unit	This work	Literature values	Reference[a]
μ_{max}	[d^{-1}]	$3.01x10^{1} \pm 1.82\ x10^{1}$	$1\ x\ 10^{1}$; $1.1\ x\ 10^{1}$; $2x10^{1}$; $1.08x10^{2}$	1,2,3,4
$K_{S,EA}$ (nitrate)	[M]	$8.18x10^{-6} \pm 4.84\ x10^{-6}$	$1.6\ x\ 10^{-6}$; $3.2\ x\ 10^{-6}$; $1.2\ x\ 10^{-5}$; $1.8\ x\ 10^{-4}$	1,3,2,4
$K_{S,ED}$ (ethanol)	[M]	$1.18x10^{-4} \pm 4.55\ x10^{-5}$	$8.3\ x\ 10^{-6}$; $1.7\ x\ 10^{-4}$; $6.6x10^{-4}$; $7.3\ x10^{-2}$	1,2,3,4
b	[d^{-1}]	$1.73x10^{-1} \pm 4.66\ x10^{-2}$	$6x10^{-2}$; $1.5x10^{-1}$; $2x10^{-1}$	2,4,3

[a] References are 1, Chen and MacQuarrie (2004); 2, Lee et al., (2009); 3, Kinzelbach et al., (1991); 4, Rodríguez-Escales et al., (2014).

Table5

Click here to download Table: Table5_v2.docx

Authors	Feeding strategy	Sediment	Time of feeding strategy (d)	Biological process	Organic carbon inflow (mM C)	Velocity (m/d)	α/α_0 (observed time)
This work	Weekly	Sand (0.5-0.8 mm)	100	Denitrification using ethanol	260-235	0.5	1 (100 d)
	Daily		200		14-35		7 (200 d)
Taylor and Jaffé (1990) and Taylor et al. (1990)	Continuous	Sand	284	Methanol oxidation (aerobic conditions)	0.22	27.2	100-1000
			356		0.17	9.1	100-1000
Bielefeldt et al. (2002)	Continuous	Sand (0.32 mm)	50	Naphthalene degradation (aerobic conditions)	1.6	3.3	1.8 (25-46)
						7.5	3-4.8 (37-44)
						11.2	2.2 (32-50)
Seifert and Engesgaard (2007)	Continuous	Sand (0.4-0.8 mm)	150	Acetate oxidation (aerobic conditions)	0.15	5.1	2 (13 d)
							7 (45 d)
Delay et al. (2013)	Continuous	Coarse crushed limestone (2 cm)	1.4	Denitrification using ethanol	1.52	34.6	1 (1.4 d)
					2.23	138.2	1 (1.4 d)